PAPER

Check for updates

A density functional study of the photocatalytic degradation of polycaprolactone by the decatungstate anion in acetonitrile solution†

Noriyuki Minezawa, [ID] [a] Kosuke Suzuki [ID] [b] and Susumu Okazaki*[a]

A recent experimental study has reported that decatungstate $[W_{10}O_{32}]^{4-}$ can degrade various polyesters in the presence of light and molecular oxygen [Li *et al.*, *Nanoscale*, 2023, **15**, 15038]. We apply density functional theory to the photocatalyst–polycaprolactone model complex in acetonitrile solution and elucidate the degradation mechanisms and catalytic cycle. We consider hydrogen atom transfer (HAT) and single electron transfer (SET) mechanisms. The potential energy profiles show that the former proceeds exergonically in a single step but that the latter involves a subsequent proton transfer and finally yields HAT products as well. Oxygenated polymer species can regain the transferred hydrogen and regenerate the reduced photocatalyst. We propose a photocatalytic cycle that realizes both the photocatalyst regeneration and the polymer degradation.

Introduction

Polyoxometalates (POMs) are a unique class of nano-scale anionic metal-oxide clusters that adopt versatile structures. By introducing several metal atoms together, one can design a variety of novel POMs and precisely manipulate their properties, such as redox potentials, acid–base strengths, absorption bands, and electronic structures. The decatungstate, $W_{10}O_{32}^{4-}$ (hereafter referred to as W10), has been studied for its potential as a photocatalyst in organic synthesis reactions[1–10] such as the functionalization of C–H bonds, the functional group transformations, and the oxidation of substrates.

Photocatalytic processes utilizing sunlight and atmospheric molecular oxygen are environmentally benign for degrading pollutants and waste materials. With this background, POMs have been used to solve environmental problems.[11] For example, the sodium salt of W10 can degrade aqueous pollutants such as pesticides.[12–14] Along with these chemicals, plastics dumped or leaked into the ocean pose urgent problems. Li *et al.*[15] have shown that POM photocatalysts, specifically W10, efficiently degrade various polyesters and polyethers under sunlight and air. These authors conducted several control experiments and found that polymer degradation mediated by W10 required light and molecular oxygen.

The photocatalytic activity of W10 has been studied extensively by time-resolved techniques, kinetic measurements, and computational methods.[16–28] These studies suggest that excited-state transient species called "wO" plays an essential role. The light absorption promotes the W10 to the ligand-to-metal charge-transfer excited state, which decays within 30–50 ps to form the reactive intermediate wO with possibly triplet multiplicity. This species persists sufficiently long (55–77 ns) and shows the characteristic absorption maximum near 780 nm. The reaction between wO and substrates proceeds by either hydrogen atom transfer (HAT)[10,19,21,29,30] or single electron transfer (SET).[20] The HAT mechanism is presumably dominant over SET, but the extent of the contribution of the latter depends on the oxidation potential of W10 (+2.44 V *vs.* SCE[28]) and substrates.

A recent study conducted by Musgrave *et al.*[31] has shown that the W10 can generate chlorine radicals from chloride ions in the photochemical partial oxidation of methane. Using the experimental techniques and density functional theory (DFT) calculations, these authors argued the chlorine radical formation by the SET mechanism and the methane conversion by halogen radicals. They also presented the energy profile of the HAT reaction between W10 and methane and that of the reoxidation of reduced W10 by molecular oxygen.

In the present work, we theoretically investigate the reaction mechanisms of polymer degradation by a W10 photocatalyst. To this end, we analyse the energy profiles of the lowest triplet state of a W10–model polycaprolactone (PCL) complex by the

a Department of Applied Materials Science, Graduate School of Frontier Sciences, The University of Tokyo, 5-1-5 Kashiwanoha, Chiba 277-8589, Japan. E-mail: okazaki@edu.k.u-tokyo.ac.jp

b Department of Applied Chemistry, School of Engineering, The University of Tokyo, 7-3-1 Hongo, Bunkyo-ku, Tokyo 113-8656, Japan

† Electronic supplementary information (ESI) available: Potential energies and Gibbs free energies of the reactions of the photocatalyst–polymer system. See DOI: https://doi.org/10.1039/d4cp00362d

DFT method and discuss (1) HAT reactions, (2) the reoxidation of reduced W10 by oxygenated species, and (3) SET reactions. We discuss these reaction mechanisms based on Gibbs free energies, potential energy profiles along the reaction coordinate, and reaction paths by the string method. Finally, we propose a photocatalytic cycle of the W10–polymer system based on the computational results. This work is the first step toward understanding recently reported multi-stimuli-responsive polymer degradation by a POM photocatalyst.[32]

Computational details

Fig. 1 presents the molecular structures of W10 and model PCL. The PCL was truncated to a dimer. Although the phenomena associated with the polymer structure, such as folding and entanglement, may affect the kinetics, the present study focuses on the chemical reactions at the local sites. The DFT calculations were performed using the ORCA program suite.[33] We considered the lowest triplet-state minimum (W10*) as a putative reactive intermediate (wO) mentioned in Introduction. The lowest triplet state was considered using an unrestricted DFT approach. We monitored the spin contamination and confirmed that the deviation from the ideal value of the triplet state (2.0) was moderate (see Tables in the ESI† for detailed values) Therefore, the multi-reference character is not severe, at least for the potential energy surfaces explored in this study.

The tetrabutylammonium cations used in the experiments were replaced with sodium ions. Indeed, the sodium salt of W10 can also degrade the polymers in water.[15] It is important to note that sodium ions do not adequately present bulky substituent effects. Not only the reaction itself, but also the association/dissociation process is essential for realizing catalytic activity. We assumed that cations merely offer a positive electrostatic field during the reaction and studied the reactions from the energetic viewpoint. We cannot exclude the possibility that kinetics controls the overall process; the bulky cations prevent polymer chains from approaching the reactive site. One must apply the molecular dynamics simulation to examine if the complexation already occurs in the ground state before the light irradiation and if the diffusional time scale matches the lifetime of the photocatalyst.

A hybrid functional based on the pure Perdew–Burke–Ernzerhof functional[34–36] was adopted, and the dispersion interaction was considered using the atom-pairwise correction with the Becke–Johnson damping scheme (PBE0-D3BJ).[37,38] An

extensive benchmark study of 200 functionals and 5000 data points shows that PBE0-D3BJ might not be accurate enough for thermochemistry.[63] To investigate how the thermodynamical data varied with density functionals, we analysed the hydrogen abstraction reaction using several functionals from pure generalized gradient approximation (GGA) to range-separated hybrid meta-GGA (see Section S1 and Fig. S1 in the ESI† for details). PBE0-D3BJ yielded the reaction energy of −28.5 kcal mol^{-1}, in comparison to −30.0 kcal mol^{-1} yielded by the most promising functional suggested in ref. 63. Despite a limited number of test calculations, the result is encouraging. The def2-SVP basis set[39] was used in the geometry optimization. More extended basis sets were used for the final single-point energy calculations: def2-TZVP[39] for H, W, and Na atoms and minimally augmented def2-TZVP (ma-def2-TZV)[39,40] for C and O atoms. For the solvent acetonitrile, a conductor-like polarizable continuum model was used. The transition state was determined by the saddle-point optimization or the nudged elastic band (NEB) method.[41,42] The thermochemical data were estimated at the temperature of 298.15 K. A quasi-rigid rotor harmonic oscillator approach was applied to evaluate the vibrational entropy due to the floppy and flexible nature of the model PCL polymer.[64] The Gibbs free energies reported are the corrected values.

Results and discussion

We discuss the reaction mechanisms based on Gibbs free energies, potential energy profiles along the reaction coordinate, and reaction paths by the string method. See Tables in the ESI† for detailed thermochemical data, potential energies at relevant geometries, and reaction schemes.

Thermodynamics

First, we examined which oxygen site is the most favorable for the HAT process. In D_{4h} symmetry, W10 has six non-equivalent oxygen atoms. The lowest-triplet minimum (W10*) was considered as a putative reactive intermediate (wO). Fig. S2 in the ESI† shows the Gibbs free energies of the α-hydrogen abstraction, W10* + PCL–H$_\alpha$ → H–W10$^\bullet$ + PCL$_\alpha^\bullet$. All values are negative (−20 to −35 kcal mol^{-1}), indicating that the HAT reaction is highly exergonic. Thus, any oxygen can accept a hydrogen atom. The formation of carbon-centered radicals is consistent with the experiments where radical scavengers significantly suppressed the degradation rate of PCL.[15] The reaction free energy of the bridge oxygen (O$_b$) has a negative number with the maximum absolute value (−34.7 kcal mol^{-1}), making this site the most favorable hydrogen acceptor. Musgrave et al.[31] reported that this site has the second-best hydrogen binding energy (lower by 0.4 kcal mol^{-1} than the best) and is easily accessible. Therefore, we selected the bridge site as the primary reaction site in this study.

Fig. 2 shows energy diagrams of the photochemical processes, and Table 1 summarizes the Gibbs free energies of the individual reactions. We considered all positions (alpha to epsilon) and tentatively assumed that the products are the
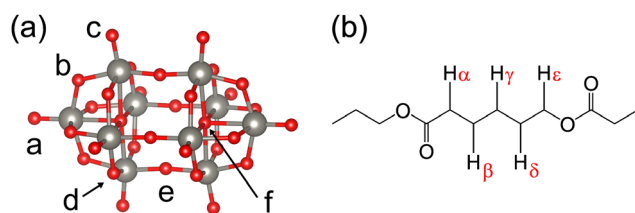

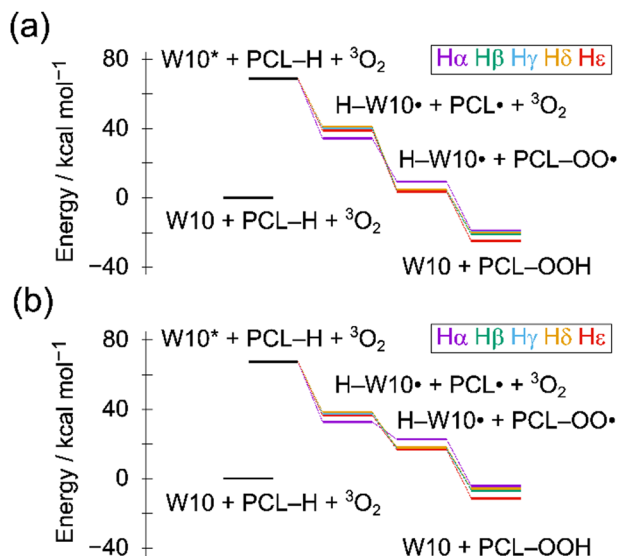Fig. 1 Molecular structures of (a) W10 and (b) model PCL: W (grey) and O (red) atoms.

This journal is © the Owner Societies 2024

Phys. Chem. Chem. Phys., 2024, **26**, 11746–11754 | **11747**

Fig. 2 Photochemical reaction profiles: (a) potential energies (without the zero-point energy correction) and (b) Gibbs free energies at 298.15 K. Relative energies (kcal mol^{-1}) of the reactants in the ground state.

regenerated W10 and PCL–OOH. Hydroperoxide species appear as an intermediate in the photo-oxidation of adamantane and cyclohexane.[21,43–45] The PCL degradation products observed in ^{1}H-NMR include hydroxy, formate, formyl, and carboxyl groups,[15] suggesting the presence of hydroperoxide intermediates. Direct hydrogen abstraction by the ground-state W10 is significantly unfavorable ($\sim$30 kcal mol^{-1}), and the result is consistent with the experimental observation that polymer degradation does not proceed without light.

Upon the photoexcitation of W10, the three processes proceed exergonically: (1) HAT from PCL to W10*, (2) formation of PCL–OO$^{\bullet}$, and (3) formation of PCL–OOH and ground-state W10. The epsilon site is the most favorable in the overall reaction. In step (1), the α-hydrogen is the most favored site due to the adjacent carbonyl group, while the subsequent process is slightly unfavorable. The energy released in the HAT process is large ($\sim$30 kcal mol^{-1}), allowing efficient reactions of the PCL radicals produced. The reaction with molecular oxygen, step (2), is highly exergonic (< -10 kcal mol^{-1}). In contrast, a radical propagation reaction, PCL$^{\bullet}$ + PCL–H → PCL–H + PCL$^{\bullet}$, leads to polymer breakage, but the process is slightly unfavorable (0–6 kcal mol^{-1}). In step (3), PCL–OO$^{\bullet}$ abstracts the hydrogen from H–W10$^{\bullet}$ and yields the ground-state W10 and PCL–OOH, completing the photocatalytic cycle. Although O$_2$-mediated oxidation, H–W10$^{\bullet}$ + ^{3}O$_2$ → W10 + HOO$^{\bullet}$, is

potentially competitive (+3.3 kcal mol^{-1}), oxygen-based radicals are not the main reactive species as shown by the experiment using radical scavengers.[15] Molecular oxygen plays an essential role in the decomposition of PCL, both in the (hydro)peroxide formation and in the regeneration of W10, which is consistent with the experimental results that the degradation does not proceed without molecular oxygen.[15]

HAT reactions of the W10–PCL complex

Fig. 3 shows the reaction energy profile of the W10–PCL complex. The results are consistent with the thermodynamics discussed above. The HAT from the PCL to W10* proceeds exothermically, and the α-hydrogen is the most reactive. The barrier height of the HAT reaction ranges from less than 1 kcal mol^{-1} (gamma and delta) to 5.5 kcal mol^{-1} (alpha), indicating that the HAT reaction occurs without difficulty and yields PCL radicals. The presence of radical species is consistent with the experiment where the radical scavenger significantly suppressed the degradation rate of PCL.[15] Interestingly, the reaction at the alpha position has the highest barrier despite the largest exothermicity. The experiments have pointed out the low reactivity at the α-carbon site.[6,7] Synergetic control by polar and steric effects plays a vital role in the site-selective C–H functionalization by W10[6,7] and the unusual regioselectivity upon aromatic hydroxylation by a divanadium-substituted γ-Keggin POM.[46] Such selectivity is due to the formation of highly electrophilic oxygen centers with partial radical character of the photoactive state of W10. As shown by the DFT calculations,[32] the α-C–H bond is the weakest, but the transition state is polarity mismatched due to the adjacent electron-withdrawing carbonyl group. Besides, steric repulsion may have some effect on the reactivity of the alpha position. The adjacent carbonyl group repels the terminal oxygen sites (a and c). After the HAT reaction, a conformational change occurs due to the interaction of the transferred hydrogen with the polar oxygen atoms in PCL. The weak interaction with the radical center (C$^{\bullet}$$\cdots$H–OW) changes to a hydrogen bond with an alkoxy (O=CO$\cdots$H–OW) or a carbonyl (OC=O$\cdots$H–OW) group.

We investigated whether the PCL radicals further react with the reduced catalyst H–W10$^{\bullet}$. Here, we addressed the hydroxylation reaction based on the rebound mechanism proposed for cytochrome P-450.[47,48] Preliminary calculations suggest that this reaction may play some role in the recently reported photocatalytic multi-stimuli-responsive polymer degradation.[32] The reaction of the HAT product is severely endergonic for the alpha position or marginally exergonic for the others, and the barrier

Table 1 Gibbs free energies (298.15 K) of photochemical processes shown in Fig. 2(b). Units: kcal mol^{-1}

Reactions	α	β	γ	δ	ε
W10 + PCL–H → H–W10$^{\bullet}$ + PCL$^{\bullet}$	32.8	37.7	37.5	38.4	36.5
W10* + PCL–H → H–W10$^{\bullet}$ + PCL$^{\bullet}$	−34.7	−29.8	−30.0	−29.2	−31.1
PCL–OO$^{\bullet}$ + H–W10$^{\bullet}$ → PCL–OOH + W10	−27.0	−24.1	−22.7	−23.8	−27.9
PCL$^{\bullet}$ + PCL–H$_\alpha$ → PCL–H + PCL$_\alpha$$^{\bullet}$	0.0	4.9	4.7	5.6	3.7
PCL$^{\bullet}$ + ^{3}O$_2$ → PCL–OO$^{\bullet}$	−10.1	−20.2	−20.6	−20.4	−19.8
PCL–OO$^{\bullet}$ + PCL–H$_\alpha$ → PCL–OOH + PCL$_\alpha$$^{\bullet}$	5.8	8.7	10.1	9.1	5.0

11748 | *Phys. Chem. Chem. Phys.*, 2024, **26**, 11746–11754

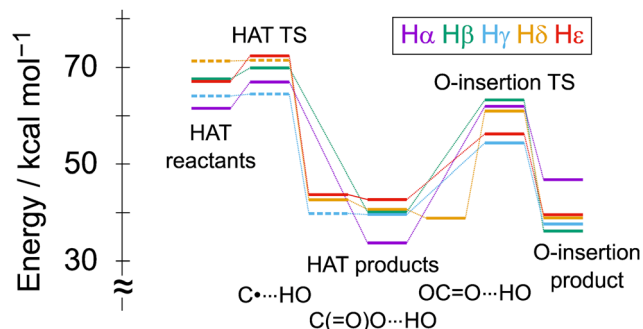This journal is © the Owner Societies 2024

Fig. 3 Potential energy (without zero-point energy correction) profiles. Relative energies (kcal mol^{-1}) of the ground-state complex. The transition states are saddle points (HAT) and energy maxima on the NEB path (oxygen insertion). The energy levels shown by dashed lines were taken from the minimum and maximum of final single-point energy calculations at the scanned geometries because the geometry optimization did not yield the corresponding geometry.

height is relatively large, 14–28 kcal mol^{-1} (Fig. 3 and Table S3 in the ESI†). In addition, the escape of the PCL radical from the HAT product complex also requires 14–20 kcal mol^{-1} (Table S3, ESI†). Therefore, polymer radicals stay in the complex long enough to decompose intramolecularly or react with molecules other than H–W10•.

Fig. 4 exemplifies the potential energy curves and the associated spin density maps for the reaction at the gamma position. We studied four representative structures (**HT1**–**HT4**). The first reaction is the HAT from PCL to HAT. In the geometry optimization, a guess reactant complex relaxed spontaneously to form product **HT2**. Note that the shallow minimum (**HT1**)

and small barrier connecting **HT1** and **HT2** appeared only in the final single-point energy calculations. For **HT1**, the two unpaired electrons are in the catalyst moiety. For the HAT product, **HT2**, one of the two unpaired electrons is at the γ-carbon of PCL, and the other delocalizes over the tungsten atoms. An early transition state for the HAT reaction is consistent with the experiments on the oxygenation of aromatic alcohols.[17] Intermediate **HT2** is not a true minimum because it has one small imaginary mode, the H–O–W bond angle. A slight displacement along that mode led to another product, **HT3**, where the transferred hydrogen interacts with the alkoxy oxygen. Despite the unsuitable reaction coordinate, there is a negligible barrier between **HT2** and **HT3** [Fig. 4(a)]. Thus, the conformational change between **HT2** and **HT3** proceeds without problems, and the overall HAT from the reactants through **HT3** works efficiently. The second reaction is hydroxylation, *i.e.*, the bond formation between the radical-center carbon and bridge oxygen atoms. Product **HT4** is PCL–OH and W10 with a defect. The two unpaired electrons delocalize over the eight equatorial tungsten atoms. The single point energy calculations on the NEB path yielded an approximate barrier of 14.7 kcal mol^{-1} from **HT3** [Fig. 4(b)], implying that this reaction is slow. Hence, **HT3** can be a reactive intermediate with a nonnegligible lifetime.

Reoxidation of reduced W10 by molecular oxygen

As discussed, the hydroxylation reaction between the PCL radical and H–W10• appears to be inefficient. We studied the reaction with molecular oxygen instead. The initial state assumed is the molecular oxygen $^3O_2$ (↑↑) and the triplet radical pair PCL (↓)···H–W10 (↓). We applied the broken-spin DFT and
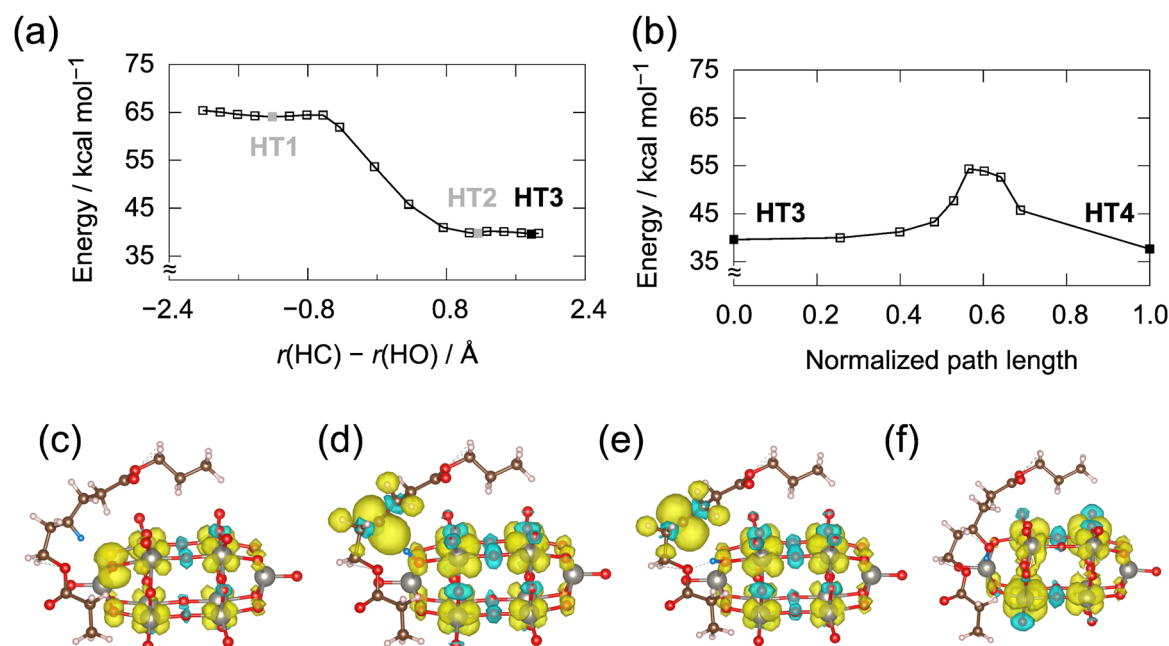

Fig. 4 Potential energy profiles of the reactions at the gamma position: (a) hydrogen abstraction by relaxed surface scan and (b) oxygen insertion by the NEB method. Relative energies (kcal mol^{-1}) of the ground-state complex. **HT1** and **HT2** are not true minima (see text). Spin density distribution at (c) **HT1**, (d) **HT2**, (e) **HT3**, and (f) **HT4**: C (brown), O (red), W (gray), and H (white). The transferred hydrogen is in blue. Positive spin surface (more spin-up electrons) is in yellow, and negative (more spin-down electrons) in cyan. Iso-surface level is 0.003 for (c) and 0.002 for (d)–(f).

This journal is © the Owner Societies 2024

Phys. Chem. Chem. Phys., 2024, **26**, 11746–11754 | **11749**

analyzed the reaction at the alpha position. Note that the α-radical is unfavorable by about 10 kcal mol^{-1} compared to the others (see −10.1 kcal mol^{-1} in Table 1). Fig. 5 shows the potential energy profiles and the spin density distributions in the reaction with molecular oxygen. Initially, the molecular oxygen attacks the H–W10$^{\bullet}$···PCL$^{\bullet}$ complex to form the adduct (**OO1**), which is lower in energy by 2.1 kcal mol^{-1} than the infinitely separated molecules. One of the two spin-up electrons is at the α-carbon atom, and the other delocalizes over the tungsten atoms. On the other hand, the two spin-down electrons are at the molecular oxygen. The bond formation with oxygen results in the peroxide (**OO2**). The spin-up electron resides in the terminal oxygen of the peroxide, while the spin-down electron is intact in the process [Fig. 5(d)]. For the reactions from the infinitely separated reactants to **OO2**, the approximate barrier (top of the potential energy curve) is 5.3 kcal mol^{-1}, and the reaction energy is −24.3 kcal mol^{-1}. Thus, the molecular oxygen can approach the complex, and the peroxide formation is more favorable than the oxygen insertion reaction described above. Note that these results rely on the energetics, not kinetics. The diffusion of molecular oxygen does matter in the actual system because of bulky neighbors: tetrabutylammonium cations, long-chain polymers, and solvent molecules. The present calculations do not explicitly take account of the molecularity of solvation structure nor the time scale of oxygen diffusion. The classical molecular dynamics simulations on the aqueous α-Keggin POM anions pointed out the importance of the microscopic molecular details of the solvent-shared structures weakly bound to the POM anions.[49]

To abstract the hydrogen of H–W10$^{\bullet}$, the PCL–OO$^{\bullet}$ must change its conformation from **OO2** to **OO3**, where the –OO$^{\bullet}$

group points to the target hydrogen [Fig. 5(e)]. The energy difference is +6.0 kcal mol^{-1}. The hydrogen abstraction by the peroxide yields the hydroperoxide complex (**OO4**). Since neither the ground-state W10 nor PCL–OOH is a radical anymore, there is no spin density in the final product. The reaction profile of **OO3** shows a small barrier (5.2 kcal mol^{-1}) and is exothermic (−28.9 kcal mol^{-1}). The overall reaction is strongly exothermic (−47.2 kcal mol^{-1}), as is consistent with the thermodynamics (Fig. 2). Therefore, the series of reactions considered here are some of the possible mechanisms of the regeneration of the ground-state W10.

The discussion above assumes that the PCL peroxide abstracts the hydrogen from H–W10$^{\bullet}$ as proposed in the oxidation of alkanes.[25] Another possibility is that the molecular oxygen abstracts the hydrogen from H–W10$^{\bullet}$ to form the hydroperoxide $^{\bullet}$OOH as proposed for the regeneration of reduced W10 in the methane oxidation.[31] The Gibbs free energy of hydrogen abstraction, H–W10$^{\bullet}$ + ^{3}O$_{2}$ → W10 + $^{\bullet}$OOH, is slightly endergonic (+3.3 kcal mol^{-1}). The reaction is thermodynamically unfavorable compared to the scheme above (Table 1) and would provide a minor pathway. In both scenarios, the regeneration of W10 by oxygen molecules is consistent with the experimental results.[15]

SET reactions of the W10–PCL complex

The SET process represents another reaction mechanism. Fig. 6 shows the potential energy profiles of the radical ion pair (PCL$^{\bullet+}$–W10$^{\bullet-}$) and spin density maps. In the initial structure (**ET1**), the radical center of PCL$^{\bullet+}$ resides in the carbonyl oxygen.

The γ-hydrogen migration occurred spontaneously in the geometry optimization, and such reaction is known as

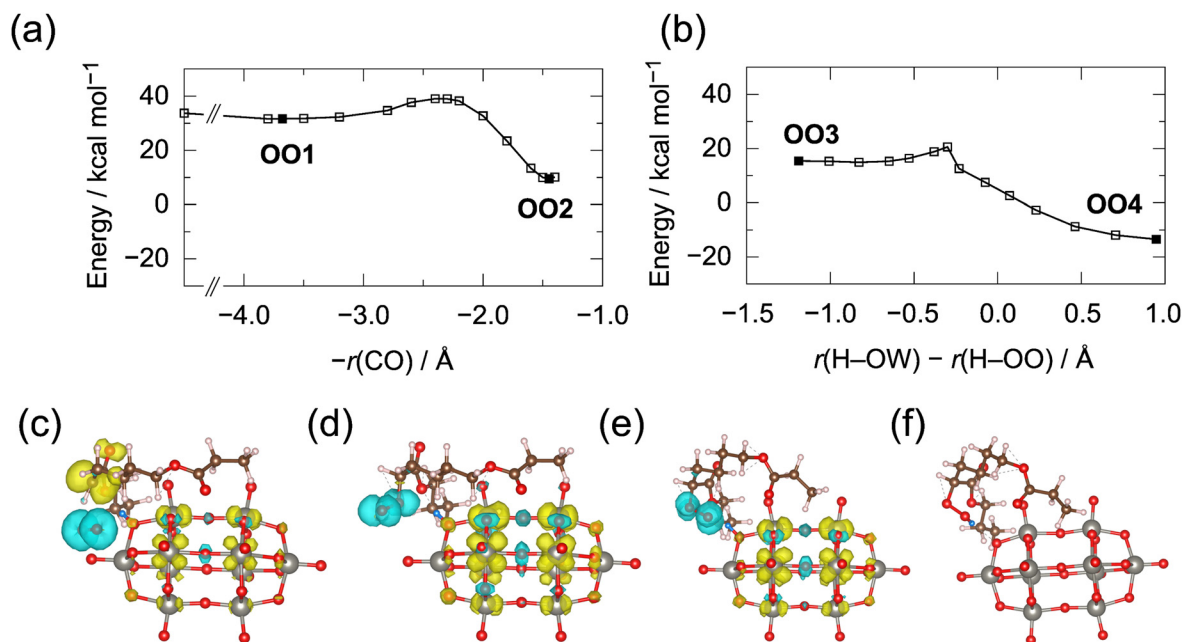**Fig. 5** Potential energy profiles of the reaction of a PCL$^{\bullet}$···H−W10$^{\bullet}$ radical pair with molecular oxygen: (a) O$_2$ approaches the carbon radical center followed by (b) hydrogen abstraction by PCL peroxide from H−W10. Relative energies (kcal mol^{-1}) of the W10−PCL complex and O$_2$ in the ground state. Spin density distribution at (c) **OO1**, (d) **OO2**, (e) **OO3**, and (f) **OO4**. The transferred hydrogen is in blue. Positive spin surface (more spin-up electrons) is in yellow, and negative (more spin-down electrons) in cyan. Iso-surface level is 0.005 for (c) and 0.003 for (d)−(f).
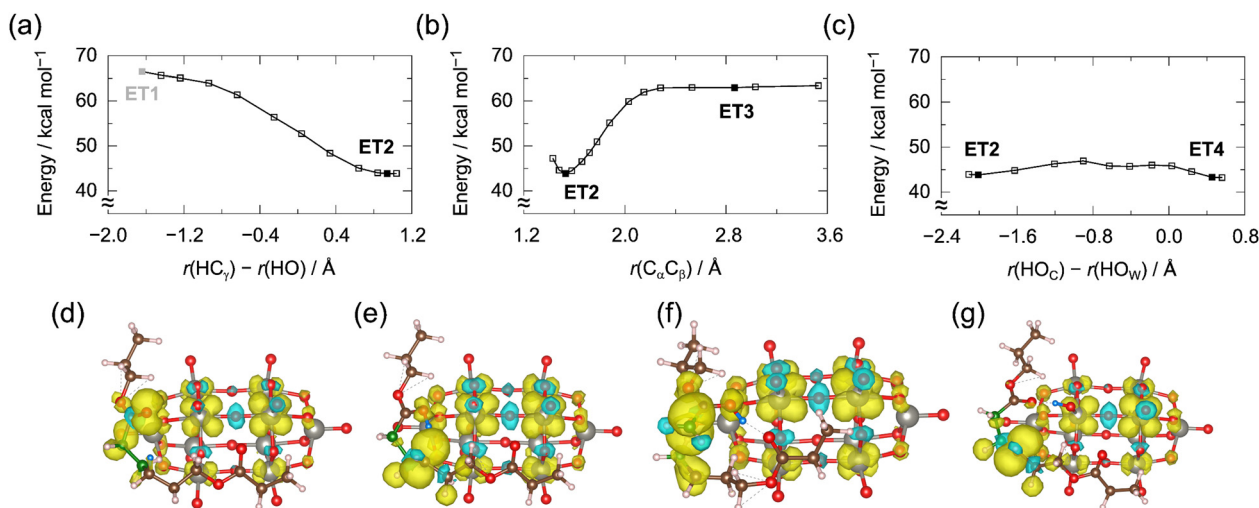
11750 | *Phys. Chem. Chem. Phys.*, 2024, **26**, 11746–11754

This journal is © the Owner Societies 2024

Fig. 6 Potential energy profiles of a PCL$^{\bullet+}$–W10$^{\bullet-}$ radical ion pair for (a) γ-hydrogen abstraction, (b) β-cleavage, and (c) proton transfer from the enol radical cation to the catalyst anion radical. Relative energies (kcal mol^{-1}) of the ground-state complex. Spin density distribution at (d) **ET1**, (e) **ET2**, (f) **ET3**, and (g) **ET4**. Note that **ET1** is not a minimum. The α- and β-carbon atoms are in green, and the transferred hydrogen in blue. Positive spin surface (more spin-up electrons) is in yellow, and negative (more spin-down electrons) in cyan. Iso-surface level is 0.003 for (d) and 0.002 for (e)–(g).

McLafferty rearrangement[50–52] observed in the carbonyl radical cation. In the product radical ion pair (**ET2**), one unpaired electron is at the γ-carbon atom, and the other delocalizes over the tungsten atoms. We could not determine the path to **ET1** because the energy increased monotonically in the relaxed surface scan. The energy of **ET1** is about 65 kcal mol^{-1} and comparable to those of HAT reactant complexes (Fig. 3). These energy levels suggest that either (1) the SET reactant minimum, if it exists, is higher in energy than that of the HAT reactant or (2) the bifurcation between the HAT and SET processes occurs at an early stage. To rationalize the branching mechanism, one must apply methods beyond the ground-state DFT and explicitly consider multiple electronic states. The DFT calculations for the lowest state show that the carbonyl oxygen radical spontaneously abstracts the γ-hydrogen once the complex switches to the charge-transfer state.

According to the McLafferty rearrangement, we examined the possibility of β-cleavage. As shown in Fig. 6(b), the energy curve along the C$_\alpha$–C$_\beta$ bond rises sharply, and the energy of the product alkene (**ET3**) is comparable to that of **ET1**. The Gibbs free energy of the reaction from **ET2** to **ET3** is highly endergonic (+16.8 kcal mol^{-1}), and such a reaction does not appear to be an efficient route.

We investigated another reaction channel involving the PT from the PCL enol radical cation to the W10 anion radical (**ET4**). The reaction involves SET followed by PT, and this two-step reaction is equivalent to HAT. Fig. 6(c) shows the energy profile along the PT reaction. We chose the terminal oxygen (O$_c$) as the proton acceptor [Fig. 6(g)]. The O$_c$ site is closer to the target proton than the bridge oxygen (O$_b$), though the former is less favorable by 8.2 kcal mol^{-1} than the latter (Fig. S2, ESI†). We obtained an approximate barrier height of 3.1 kcal mol^{-1} by a relaxed surface scan along the reaction coordinate. If the radical ion pair adopts the conformation where the migrating proton is closer to the bridge oxygen, the reaction would be more exothermic, and the barrier height would decrease further.

Summary of degradation mechanisms

Fig. 7 summarizes the polymer degradation mechanisms based on the experiments and present calculations. The photo-excited W10 abstracts the hydrogen from PCL by either single-step HAT or two-step HAT (SET followed by PT). The PCL radical triggers chain reactions leading to polymer degradation or combines with molecular oxygen to form peroxide. The peroxide initializes radical propagation or regenerates the ground-state W10 by the hydrogen abstraction from the reduced catalyst (H–W10$^{\bullet}$). The proposed cycle is consistent with the experiment:[15] (1) the photocatalyst, light, and molecular oxygen are essential; (2) the carbon-centred radicals are formed; and (3) oxygen-based radicals play a minor role.

The remaining question is how polymer radicals decompose. The discussion so far is focused on the photo-oxidation of PCL, not the photo-degradation. To accelerate the degradation of polyesters, the bond cleavage or hydrolysis in the main chain must occur. Ref. 53 has reviewed the degradation mechanisms relevant to PCL: radical-mediated, thermal, or enzymatic degradation. As discussed in Section 3.2, the PCL radicals persist long enough as the HAT product complex. When the intersystem crossing occurs, the recovery of the ground-state W10 by
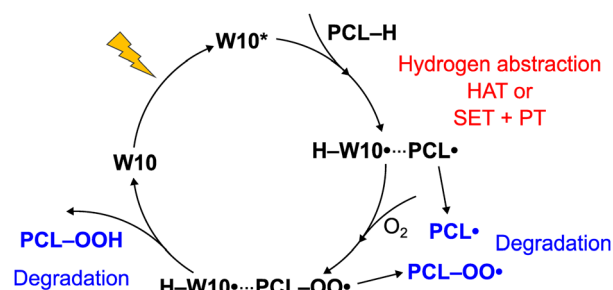

Fig. 7 Proposed photocatalytic cycle of the W10–PCL system.

This journal is © the Owner Societies 2024

Phys. Chem. Chem. Phys., 2024, **26**, 11746–11754 | **11751**

the reverse HAT reaction is strongly exergonic (see the first reaction in Table 1). Besides, leaving the complex requires considerable energy (14–20 kcal mol^{-1}). Thus, the role of free PCL radicals appears to be minor. Fig. S4 (ESI†) shows the Gibbs free energies of the β-cleavage of PCL radicals. We found that the ε-radical is the most labile (+6.4 kcal mol^{-1}) and that the bond dissociation can compete with the radical propagation (Table 1). Besides, the formation of stable CO_2 by decarboxylation is a thermodynamical driving force, and the free energies of decomposition are −7.4 and −8.8 kcal mol^{-1} for the beta and delta sites, respectively. From a thermodynamic point of view, these paths may contribute to the polymer degradation.

The final product of this cycle is hydroperoxide. The subsequent reactions of this species have been proposed.[31] Hydrogen peroxide is the product of the sequential removal of hydrogen by molecular oxygen from the two reduced W10, $O_2 \rightarrow {}^\bullet OOH \rightarrow HOOH$. The generated HOOH reacts with (a) the hydroxy radical, $HOOH + {}^\bullet OH \rightarrow {}^\bullet OOH + H_2O$, or (b) hydroperoxide, $HOOH + {}^\bullet OOH \rightarrow {}^\bullet OH + H_2O + {}^3O_2$. Following these mechanisms for HOOH, we computed the Gibbs free energies of putative reactions of PCL–OOH (Table S4, ESI†). The reactions with H–W10$^\bullet$, $^\bullet OH$, $^\bullet OOH$, and PCL–OO$^\bullet$ are all exergonic. The alkoxy radicals (PCL–O$^\bullet$) generated are highly reactive intermediates, and several reactions are conceivable: recombination (dimerization), hydrogen abstraction, addition to double bonds, rearrangement, bond fission, and disproportion.[54,55] The hydrogen abstraction deactivates the radical and yields the hydroxylated product (PCL–OH). The experiment has detected the hydroxy group.[15] The β-cleavage of alkoxy radicals is one of the reaction mechanisms considered in the context of photochemical polymer degradation.[56–58] Fig. S5 (ESI†) shows the Gibbs free energies of the β-cleavage of PCL–O$^\bullet$ radicals. These radicals decompose more efficiently than the PCL alkyl radicals as shown in Fig. S4 (ESI†). Most reactions are exergonic, and the formation of aldehydes agrees with the experiment.[15]

Conclusions

In the present work, we examined the polymer degradation mechanisms by the W10 photocatalyst using density functional theory. The conclusions derived from the calculations are as follows:

- W10 in the lowest triplet state can abstract any hydrogen from PCL. The reaction is highly exothermic, and the barrier height is low enough.
- PCL radicals (a) react with molecular oxygen and form PCL–OO$^\bullet$ or (b) undergo radical propagation and decomposition.
- PCL–OO$^\bullet$ can abstract the hydrogen from H–W10$^\bullet$ and regenerate the ground-state W10. Thus, molecular oxygen plays an essential role in maintaining the photocatalytic activity of W10.
- SET reaction promotes the γ-hydrogen abstraction of the PCL radical cation, but subsequent β-cleavage is highly endergonic. In contrast, the PT reaction has a sufficiently

small barrier and allows a two-step process (SET followed by PT) equivalent to HAT. The contribution of the SET mechanism will depend on the redox potential of substrate polymers, as suggested by the experiment.[20,22,27]

This study did not answer how the bifurcation between HAT and SET occurs and what factors control it. Since the SET reaction involves multiple potential surfaces, one must explore crossings, reaction paths, and barriers using elaborate electronic structure methods.[28,59,60] Another direction is to monitor the whole photochemical processes on the fly using the molecular dynamics simulation with multiple electronic states.[61,62]

Finally, it will be interesting to see how far this study can explain the degradation of other polymers. For example, polyethylene terephthalate (PET) has been used extensively in real life. Since the photo-oxygenation of the aromatic hydrocarbons and alcohols proceeds *via* the HAT mechanism,[16–18] the present results would hold for PET. Polyethers such as polyethyleneglycol and polytetrahydrofuran are polymers that W10 can degrade.[15] Since the oxidation potential of polyethers is lower than that of polyesters, SET will have an appreciable impact on the degradation. The present calculations provide valuable insights into the development of environmentally friendly POM photocatalysts for polymer degradation.

Conflicts of interest

There are no conflicts to declare.

Acknowledgements

References

1 S.-S. Wang and G.-Y. Yang, Recent Advances in Polyoxometalate-Catalyzed Reactions, *Chem. Rev.*, 2015, **115**, 4893–4962.

2 D. Ravelli, S. Protti and M. Fagnoni, Decatungstate Anion for Photocatalyzed "Window Ledge" Reactions, *Acc. Chem. Res.*, 2016, **49**, 2232–2242.

3 K. Suzuki, N. Mizuno and K. Yamaguchi, Polyoxometalate Photocatalysis for Liquid-Phase Selective Organic Functional Group Transformations, *ACS Catal.*, 2018, **8**, 10809–10825.

4 L. Capaldo, D. Ravelli and M. Fagnoni, Direct Photocatalyzed Hydrogen Atom Transfer (HAT) for Aliphatic C–H Bonds Elaboration, *Chem. Rev.*, 2022, **122**, 1875–1924.

11752 | *Phys. Chem. Chem. Phys.*, 2024, **26**, 11746–11754

This journal is © the Owner Societies 2024

5 N. Holmberg-Douglas and D. A. Nicewicz, Photoredox-Catalyzed C–H Functionalization Reactions, *Chem. Rev.*, 2022, **122**, 1925–2016.

6 D. Ravelli, M. Fagnoni, T. Fukuyama, T. Nishikawa and I. Ryu, Site-Selective C–H Functionalization by Decatungstate Anion Photocatalysis: Synergistic Control by Polar and Steric Effects Expands the Reaction Scope, *ACS Catal.*, 2018, **8**, 701–713.

7 K. Yamada, T. Fukuyama, S. Fujii, D. Ravelli, M. Fagnoni and I. Ryu, Cooperative Polar/Steric Strategy in Achieving Site-Selective Photocatalyzed C(sp3)–H Functionalization, *Chem. – Eur. J.*, 2017, **23**, 8615–8618.

8 M. D. Tzirakis, I. N. Lykakis and M. Orfanopoulos, Decatungstate as an efficient photocatalyst in organic chemistry, *Chem. Soc. Rev.*, 2009, **38**, 2609–2621.

9 M. Fagnoni, D. Dondi, D. Ravelli and A. Albini, Photocatalysis for the Formation of the C–C Bond, *Chem. Rev.*, 2007, **107**, 2725–2756.

10 G. Laudadio, Y. Deng, K. Van Der Wal, D. Ravelli, M. Nuño, M. Fagnoni, D. Guthrie, Y. Sun and T. Noël, C(sp^3)–H functionalizations of light hydrocarbons using decatungstate photocatalysis in flow, *Science*, 2020, **369**, 92–96.

11 S. Omwoma, C. T. Gore, Y. Ji, C. Hu and Y.-F. Song, Environmentally benign polyoxometalate materials, *Coord. Chem. Rev.*, 2015, **286**, 17–29.

12 S. Rafqah, P. W.-W. Chung, C. Forano and M. Sarakha, Photocatalytic degradation of metsulfuron methyl in aqueous solution by decatungstate anions, *J. Photochem. Photobiol., A: Chem.*, 2008, **199**, 297–302.

13 A. Hiskia, A. Troupis, S. Antonaraki, E. Gkika and P. K. Papaconstantinou, Polyoxometallate photocatalysis for decontaminating the aquatic environment from organic and inorganic pollutants, *Int. J. Environ. Anal. Chem.*, 2006, **86**, 233–242.

14 I. Texier, C. Giannotti, S. Malato, C. Richter and J. Delaire, Solar photodegradation of pesticides in water by sodium decatungstate, *Catal. Today*, 1999, **54**, 297–307.

15 C. Li, C. Gu, K. Yamaguchi and K. Suzuki, Highly efficient degradation of polyesters and polyethers by decatungstate photocatalysis, *Nanoscale*, 2023, **15**, 15038–15042.

16 C. Tanielian, I. N. Lykakis, R. Seghrouchni, F. Cougnon and M. Orfanopoulos, Mechanism of decatungstate photocatalyzed oxygenation of aromatic alcohols Part I. Continuous photolysis and laser flash photolysis studies, *J. Mol. Catal. A: Chem.*, 2007, **262**, 170–175.

17 I. N. Lykakis, C. Tanielian, R. Seghrouchni and M. Orfanopoulos, Mechanism of decatungstate photocatalyzed oxygenation of aromatic alcohols Part II. Kinetic isotope effects studies, *J. Mol. Catal. A: Chem.*, 2007, **262**, 176–184.

18 I. N. Lykakis and M. Orfanopoulos, Deuterium kinetic isotope effects in homogeneous decatungstate catalyzed photooxygenation of 1,1-diphenylethane and 9-methyl-9H-fluorene: evidence for a hydrogen abstraction mechanism, *Tetrahedron Lett.*, 2005, **46**, 7835–7839.

19 C. Tanielian, C. Schweitzer, R. Seghrouchni, M. Esch and R. Mechin, Polyoxometalate sensitization in mechanistic studies of photochemical reactions: The decatungstate anion as a reference sensitizer for photoinduced free radical oxygenations of organic compounds, *Photochem. Photobiol. Sci.*, 2003, **2**, 297–305.

20 C. Tanielian, R. Seghrouchni and C. Schweitzer, Decatungstate Photocatalyzed Electron-Transfer Reactions of Alkenes. Interception of the Geminate Radical Ion Pair by Oxygen, *J. Phys. Chem. A*, 2003, **107**, 1102–1111.

21 C. Tanielian, K. Duffy and A. Jones, Kinetic and Mechanistic Aspects of Photocatalysis by Polyoxotungstates: A Laser Flash Photolysis, Pulse Radiolysis, and Continuous Photolysis Study, *J. Phys. Chem. B*, 1997, **101**, 4276–4282.

22 D. C. Duncan and M. A. Fox, Early Events in Decatungstate Photocatalyzed Oxidations: A Nanosecond Laser Transient Absorbance Reinvestigation, *J. Phys. Chem. A*, 1998, **102**, 4559–4567.

23 D. C. Duncan, T. L. Netzel and C. L. Hill, Early-Time Dynamics and Reactivity of Polyoxometalate Excited States. Identification of a Short-Lived LMCT Excited State and a Reactive Long-Lived Charge-Transfer Intermediate following Picosecond Flash Excitation of $[W_{10}O_{32}]^{4-}$ in Acetonitrile, *Inorg. Chem.*, 1995, **34**, 4640–4646.

24 R. F. Renneke, M. Pasquali and C. L. Hill, Polyoxometalate systems for the catalytic selective production of nonthermodynamic alkenes from alkanes. Nature of excited-state deactivation processes and control of subsequent thermal processes in polyoxometalate photoredox chemistry, *J. Am. Chem. Soc.*, 1990, **112**, 6585–6594.

25 L. P. Ermolenko, J. A. Delaire and C. Giannotti, Laser flash photolysis study of the mechanism of photooxidation of alkanes catalysed by decatungstate anion, *J. Chem. Soc., Perkin Trans. 2*, 1997, 25–30.

26 I. Texier, J.-F. Delouis, J. A. Delaire, C. Giannotti, P. Plaza and M. M. Martin, Dynamics of the first excited state of the decatungstate anion studied by subpicosecond laser spectroscopy, *Chem. Phys. Lett.*, 1999, **311**, 139–145.

27 I. Texier, J. A. Delaire and C. Giannotti, Reactivity of the charge transfer excited state of sodium decatungstate at the nanosecond time scale, *Phys. Chem. Chem. Phys.*, 2000, **2**, 1205–1212.

28 V. D. Waele, O. Poizat, M. Fagnoni, A. Bagno and D. Ravelli, Unraveling the Key Features of the Reactive State of Decatungstate Anion in Hydrogen Atom Transfer (HAT) Photocatalysis, *ACS Catal.*, 2016, **6**, 7174–7182.

29 L. Capaldo and D. Ravelli, Decatungstate as Direct Hydrogen Atom Transfer Photocatalyst for SOMOphilic Alkynylation, *Org. Lett.*, 2021, **23**, 2243–2247.

30 J. Zeng, T. Torigoe and Y. Kuninobu, Control of Site-Selectivity in Hydrogen Atom Transfer by Electrostatic Interaction: Proximal-Selective C(sp^3)–H Alkylation of 2-Methylanilinium Salts Using a Decatungstate Photocatalyst, *ACS Catal.*, 2022, **12**, 3058–3062.

31 C. B. Musgrave, K. Olsen, N. S. Liebov, J. T. Groves, W. A. Goddard and T. B. Gunnoe, Partial Oxidation of Methane Enabled by Decatungstate Photocatalysis Coupled to Free Radical Chemistry, *ACS Catal.*, 2023, **13**, 6382–6395.

This journal is © the Owner Societies 2024

Phys. Chem. Chem. Phys., 2024, **26**, 11746–11754 | 11753

32 C. Gu, C. Li, N. Minezawa, S. Okazaki, K. Yamaguchi and K. Suzuki, Multi-stimuli-responsive polymer degradation by polyoxometalate photocatalysis and chloride ion, *Nanoscale*, 2024, DOI: **10.1039/d4nr00394b**.

33 F. Neese, F. Wennmohs, U. Becker and C. Riplinger, The ORCA quantum chemistry program package, *J. Chem. Phys.*, 2020, **152**, 224108.

34 J. P. Perdew, K. Burke and M. Ernzerhof, Generalized Gradient Approximation Made Simple, *Phys. Rev. Lett.*, 1996, **77**, 3865–3868.

35 J. P. Perdew, K. Burke and M. Ernzerhof, Generalized Gradient Approximation Made Simple [Phys. Rev. Lett. 77, 3865 (1996)], *Phys. Rev. Lett.*, 1997, **78**, 1396.

36 C. Adamo and V. Barone, Toward reliable density functional methods without adjustable parameters: The PBE0 model, *J. Chem. Phys.*, 1999, **110**, 6158–6170.

37 S. Grimme, J. Antony, S. Ehrlich and H. Krieg, A consistent and accurate *ab initio* parametrization of density functional dispersion correction (DFT-D) for the 94 elements H-Pu, *J. Chem. Phys.*, 2010, **132**, 154104.

38 S. Grimme, S. Ehrlich and L. Goerigk, Effect of the damping function in dispersion corrected density functional theory, *J. Comput. Chem.*, 2011, **32**, 1456–1465.

39 F. Weigend and R. Ahlrichs, Balanced basis sets of split valence, triple zeta valence and quadruple zeta valence quality for H to Rn: Design and assessment of accuracy, *Phys. Chem. Chem. Phys.*, 2005, **7**, 3297–3305.

40 J. Zheng, X. Xu and D. G. Truhlar, Minimally augmented Karlsruhe basis sets, *Theor. Chem. Acc.*, 2011, **128**, 295–305.

41 G. Mills, H. Jónsson and G. K. Schenter, Reversible work transition state theory: application to dissociative adsorption of hydrogen, *Surf. Sci.*, 1995, **324**, 305–337.

42 G. Henkelman and H. Jónsson, Improved tangent estimate in the nudged elastic band method for finding minimum energy paths and saddle points, *J. Chem. Phys.*, 2000, **113**, 9978–9985.

43 W. Wu, Z. Fu, S. Tang, S. Zou, X. Wen, Y. Meng, S. Sun, J. Deng, Y. Liu and D. Yin, $(nBu_4N)_4W_{10}O_{32}$-catalyzed selective oxygenation of cyclohexane by molecular oxygen under visible light irradiation, *Appl. Catal., B*, 2015, **164**, 113–119.

44 C. Giannotti and C. Richter, Photocatalysed oxidation of cyclohexane by $W_{10}O_{32}{}^{4-}$ irradiation with natural sunlight, *Int. J. Photoenergy*, 1999, **1**, 69–73.

45 I. Texier, C. Giannotti, S. Malato, C. Richter, J. Ouazzani and J. Delaire, Potential applications of solar reactions photocatalysed by the decatungstate anion, *J. Chim. Phys. Phys.-Chim. Biol.*, 1999, **96**, 430–436.

46 I. Y. Skobelev, V. Yu Evtushok, O. A. Kholdeeva, N. V. Maksimchuk, R. I. Maksimovskaya, J. M. Ricart, J. M. Poblet and J. J. Carbó, Understanding the Regioselectivity of Aromatic Hydroxylation over Divanadium-Substituted γ-Keggin Polyoxotungstate, *ACS Catal.*, 2017, **7**, 8514–8523.

47 J. C. Schöneboom, S. Cohen, H. Lin, S. Shaik and W. Thiel, Quantum Mechanical/Molecular Mechanical Investigation of the Mechanism of C−H Hydroxylation of Camphor by Cytochrome P450$_{cam}$: Theory Supports a Two-State Rebound Mechanism, *J. Am. Chem. Soc.*, 2004, **126**, 4017–4034.

48 J. H. Han, S.-K. Yoo, J. S. Seo, S. J. Hong, S. K. Kim and C. Kim, Biomimetic alcohol oxidations by an iron(iii) porphyrin complex: relevance to cytochrome P-450 catalytic oxidation and involvement of the two-state radical rebound mechanism, *Dalton Trans.*, 2005, 402.

49 F. Leroy, P. Miró, J. M. Poblet and C. Bo, and J. Bonet Ávalos, Keggin Polyoxoanions in Aqueous Solution: Ion Pairing and Its Effect on Dynamic Properties by Molecular Dynamics Simulations, *J. Phys. Chem. B*, 2008, **112**, 8591–8599.

50 F. W. McLafferty, Mass Spectrometric Analysis. Molecular Rearrangements, *Anal. Chem.*, 1959, **31**, 82–87.

51 D. G. I. Kingston, J. T. Bursey and M. M. Bursey, Intramolecular hydrogen transfer in mass spectra. II. McLafferty rearrangement and related reactions, *Chem. Rev.*, 1974, **74**, 215–242.

52 J. Stamm, S. Kwon, S. Sandhu, M. Shaik, R. Das, J. Sandhu, B. Curenton, C. Wicka, B. G. Levine, L. Sun and M. Dantus, The Surprising Dynamics of the McLafferty Rearrangement, *J. Phys. Chem. Lett.*, 2023, **14**, 10088–10093.

53 M. Bartnikowski, T. R. Dargaville, S. Ivanovski and D. W. Hutmacher, Degradation mechanisms of polycaprolactone in the context of chemistry, geometry and environment, *Prog. Polym. Sci.*, 2019, **96**, 1–20.

54 L. Chang, Q. An, L. Duan, K. Feng and Z. Zuo, Alkoxy Radicals See the Light: New Paradigms of Photochemical Synthesis, *Chem. Rev.*, 2022, **122**, 2429–2486.

55 P. Gray and A. Williams, The Thermochemistry And Reactivity Of Alkoxyl Radicals, *Chem. Rev.*, 1959, **59**, 239–328.

56 Z. Huang and H. Wang, A review on photochemical effects of common plastics and their related applications, *J. Polym. Sci.*, 2024, **62**, 969–997.

57 D. M. Wiles and D. J. Carlsson, Photostabilisation mechanisms in polymers: A review, *Polym. Degrad. Stabil.*, 1980, **3**, 61–72.

58 D. J. Carlsson and D. M. Wiles, The Photodegradation of Polypropylene Films. III. Photolysis of Polypropylene Hydroperoxides, *Macromolecules*, 1969, **2**, 597–606.

59 D. Ravelli, D. Dondi, M. Fagnoni, A. Albini and A. Bagno, Electronic and EPR spectra of the species involved in $[W_{10}O_{32}]^{4-}$ photocatalysis. A relativistic DFT investigation, *Phys. Chem. Chem. Phys.*, 2013, **15**, 2890–2896.

60 D. Ravelli, D. Dondi, M. Fagnoni, A. Albini and A. Bagno, Predicting the UV spectrum of polyoxometalates by TD-DFT, *J. Comput. Chem.*, 2011, **32**, 2983–2987.

61 N. Minezawa and T. Nakajima, Trajectory surface hopping molecular dynamics simulation by spin-flip time-dependent density functional theory, *J. Chem. Phys.*, 2019, **150**, 204120.

62 N. Minezawa and T. Nakajima, Quantum mechanical/molecular mechanical trajectory surface hopping molecular dynamics simulation by spin-flip time-dependent density functional theory, *J. Chem. Phys.*, 2020, **152**, 024119.

63 N. Mardirossian and M. Head-Gordon, Thirty years of density functional theory in computational chemistry: an overview and extensive assessment of 200 density functionals, *Mol. Phys.*, 2017, **115**, 2315–2372.

64 S. Grimme, Supramolecular Binding Thermodynamics by Dispersion-Corrected Density Functional Theory, *Chem. – Eur. J.*, 2012, **18**, 9955–9964.

11754 | *Phys. Chem. Chem. Phys.*, 2024, **26**, 11746–11754

This journal is © the Owner Societies 2024